INTERNATIONAL JOURNAL FOR NUMERICAL METHODS IN FLUIDS
Int. J. Numer. Meth. Fluids 2004; **44**:1063–1091 (DOI: 10.1002/fld.668)

A time-accurate pseudo-compressibility approach based on an unstructured hybrid finite volume technique applied to unsteady turbulent premixed flame propagation

Wladimyr M. C. Dourado[1,*,†], Pascal Bruel[2] and João L. F. Azevedo[3]

[1]*Centro Técnico Aeroespacial, IAE, ASA-P São José dos Campos, SP 12228-904, Brazil*
[2]*Centre National de la Recherche Scientifique, Laboratoire de Combustion et de Détonique, ENSMA, B. P. 40109, Futuroscope 86961, France*
[3]*Centro Técnico Aeroespacial, IAE, ASE-N, São José dos Campos, SP, 12228-904, Brazil*

SUMMARY

A preconditioning approach based on the artificial compressibility formulation is extended to solve the governing equations for unsteady turbulent reactive flows with heat release, at low Mach numbers, on an unstructured hybrid grid context. Premixed reactants are considered and a flamelet approach for combustion modelling is adopted using a continuous quenched mean reaction rate. An overlapped cell-vertex finite volume method is adopted as a discretisation scheme. Artificial dissipation terms for hybrid grids are explicitly added to ensure a stable, discretised set of equations. A second-order, explicit, hybrid Runge–Kutta scheme is applied for the time marching in pseudo-time. A time derivative of the dependent variable is added to recover the time accuracy of the preconditioned set of equations. This derivative is discretised by an implicit, second-order scheme. The resulting scheme is applied to the calculation of an infinite planar (one-dimensional) turbulent premixed flame propagating freely in reactants whose turbulence is supposed to be frozen, homogeneous and isotropic. The accuracy of the results obtained with the proposed method proves to be excellent when compared to the data available in the literature.

KEY WORDS: unsteady turbulent combustion; quenched flame; finite volume method; unstructured hybrid grid; pseudo-compressibility method

1. INTRODUCTION

Unsteady and steady reactive flows with strong density variations due to heat release in combustion processes are often encountered in many system of practical interest. Yet, a large number of these applications consists of complex geometries either in terms of design or flow configuration. Non-trivial gradients distributed in irregular form throughout the domain may give an example of the flow complexity. In addition, in a large number of practical applica-

*Correspondence to: W. M. C. Dourado, Instituto de Aeronautica e Espaco, Centro Tecnico Aeroespacial, CTA/IAE/ASE-N, 12228-904 São José dos Campos, SP, Brazil.
†E-mail: wladimyrmd@terra.com.br

Received 9 November 2002
Revised 31 August 2003

tions, the flow is characterised by a very low Mach number (M) regime. For such cases, the pressure is thermodynamically constant and it depends only on the flow motion through its derivatives in the momentum equation. Furthermore, a coupling of the velocity and pressure is weakly detected by the total energy equation. Some procedures based on the solution of the Poisson equation for pressure, as presented by Karki and Patankar [1] and Chen and Pletcher [2], are applied to calculate these types of flows, but they present some drawbacks in comparison with usual compressible methods. Hence, a method which is able to inherit a large number of routines and procedures developed by a broader community is preferable. Small modifications may leave a compressible code able to treat both compressible and incompressible flows. Among the several types of methods which may serve for this purpose, the artificial compressibility (AC) method has been a well-established numerical approach for the solution of the compressible Navier–Stokes equations on very low Mach number flow regime, either for inert flows (see Reference [3]) or reactive flows (see References [4–6]). For inert flows, Dourado and Azevedo [7, 8] and Dourado *et al.* [9] have shown that some preconditioning techniques work well up to a limit in the low Mach number flow regime, e.g. $M \geqslant 0.01$.

On the other hand, finite volume, unstructured grid techniques have shown, during the last two decades, a strong versatility to treat a wide range of geometries and complex configurations in the compressible flow regime (see References [10, 11]). Localised refinement techniques are also easily employed on unstructured grids (see References [12–14]). Therefore, their use to deal with reactive flows, in which strong gradients are present throughout the domain, has clear advantages.

The main effort of the present work is to adapt a pseudo-compressibility technique, developed by one of the authors (see References [4, 6]), to very low Mach number reactive flows on a two-dimensional overlapped cell-vertex unstructured grid context. The test cases consist of both of steady and unsteady freely propagating planar flames, with appropriate boundary conditions to ensure a 1D-like mean flow properties. The results obtained with the present scheme are compared with other analytical and numerical solutions available in the literature.

2. PHYSICAL MODELLING

2.1. Combustion model

Since the present study is mainly concerned with the numerical method for the solution of the governing equations rather than the combustion modelling of the combustion process itself, only a brief description of the modelling is given here. We emphasise the fact that, thanks to its intrinsic mathematical properties, we are using the chosen turbulent combustion model to test our numerical approach in the way followed by Corvellec *et al.* [6]. Our attention here is focused on the case of highly turbulent reactive flows that can be typically found in many industrial systems such as furnaces, primary combustion chambers, turbo-machinery combustion chambers and afterburners. A large number of these flows are characterised by high density changes uniquely related to chemistry. The work adopts a thermo-chemistry mechanism given by the Bray–Moss–Libby model (BML model) for premixed combustion which assumes an isenthalpic flow with infinitely fast chemical reactions (flamelet regime of turbulent premixed combustion). More details on such a combustion regime can be found

in References [15–18]. The high Reynolds number flow upstream of the considered flame is supposed to be homogeneous and isotropic. The approach considers that the combustion process takes place in infinitely thin, laminar-like reactive interfaces (flamelets). For such a process, an observer recording the temperature signal at a given point within the flow would obtain basically two values of temperature: $T = T_b$ in the all burnt products and $T = T_r$ in the unburnt mixture. The combustion process is given by a single bi-valued progress variable c ($c = 0$ in unburnt mixture and $c = 1$ in the fully burnt products) which plays the role of a reduced temperature via the following relation:

$$c = \frac{T - T_r}{T_b - T_r} \tag{1}$$

The static pressure is thermodynamically constant as a consequence of the zero Mach number hypothesis in the sense of Majda and Sethian [19]. Hence, density variations are uniquely related to temperature changes due to the heat release. Therefore, for an isenthalpic flow, the relevant state equation relating temperature T and density ρ is given by

$$\rho T = \rho_r T_r = \rho_b T_b \tag{2}$$

With the help of the heat release parameter, χ, which characterises the gas expansion associated with the heat release and which is given by the relation

$$\chi = \frac{(T_b - T_r)}{T_r} \tag{3}$$

the state equation, Equation (2), can be rewritten in terms of the progress variable as

$$\rho = \frac{\rho_r}{1 + \chi c} \tag{4}$$

With the use of classical Favre average [20], the mean equation of state is given by

$$\bar{\rho} = \frac{\rho_r}{1 + \chi \tilde{c}} \tag{5}$$

Here, $\tilde{c}$ is the mass weighted Favre average of c defined as $\tilde{c} = \overline{\rho c}/\bar{\rho}$, where the overbar denotes the Reynolds average of the corresponding variable. With the hypothesis of unitary Lewis number, the governing equation for the mean progress variable plays the role of the energy equation and it can be written in the generic form:

$$L(\bar{\rho}\tilde{c}) = \bar{w} \tag{6}$$

where the L operator regroups the convective and diffusive operators. The mean reaction rate, $\bar{w}$, appearing in the above equation may take different forms depending on the version of the combustion model. However, as mentioned before, such details are beyond the scope of the present paper and only a brief outline of the mean reaction rate model is given here.

As mentioned previously, our primary goal here is to test our numerical approach without any ambiguity. In that respect, it has been recently shown (see, for instance, References [5, 21]), that when the analysis pioneered by Kolmogorov *et al.* [22] is applied to a quenched eddy-break-up expression of the mean reaction rate, the turbulent flame brush structure as well as its propagation velocity are unique and depend only on the quenching value. The reader

interested in the details of turbulent flame propagation will find a comprehensive survey on that topic in Reference [23]. Thus, for the evaluation of a numerical scheme, a quenched form of the mean reaction rate model appears to be a good choice since, by setting the mean reaction rate to zero, as soon as the progress variable is less than some quenching value, $c^\star$, a unique steady regime of flame propagation is selected (see also References [24, 25]).

As discussed in Reference [6], a non-continuous quenched form of $\bar{w}$ presents the drawback of introducing a non-continuous pressure gradient within the mean flame brush at the point where the progress variable reaches the quenching value $c^\star$. The adoption of a non-continuous production term $\bar{w}$ as a function of $\tilde{c}$ makes it more difficult to test the numerical scheme which is always mesh refinement sensitive in the vicinity of the pressure gradient discontinuity. Therefore, a continuous quenched form of the mean reaction rate, $\bar{w}$, is used in the present study, which is given by

$$\bar{w} = \begin{cases} 0, & \text{if } \tilde{c} \leqslant \chi c^\star \\ C_w(1+\chi)\dfrac{(\tilde{c}-\chi c^\star)(1-\tilde{c})}{(1+\chi c^\star)^2}, & \text{otherwise} \end{cases} \tag{7}$$

where C_w is a constant. The recourse to such an expression of $\bar{w}$ ensures that mean flame brush can propagate steadily with one and only one value of the propagation velocity that we shall call S_{t_0} that can be thought of as being the 'model intrinsic' propagation velocity which is a constant as soon as χ and $c^\star$ are prescribed.

As explained in the next sections, the spatial discretisation of the governing equations, adopted here, is a cell-vertex finite-volume formulation using the trapezoidal rule of integration. This is quite different from the approach used in Reference [6], in which the spatial discretisation is essentially structured and fluxes are computed through the use of staggered grids. Therefore, in the present work, the source term is treated in a simpler, way different, from that presented by Corvellec [6], and it is not given in split form as in that work.

2.2. *Pseudo-compressibility technique*

Different methods have been presented in the literature to solve the Navier–Stokes equations in a constant density regime. As presented by Soh and Goodrich [26], a considerable difficulty for incompressible flow calculations is associated with the fact that the continuity equation is in divergence-free form, and its calculation is not time dependent. Furthermore, pressure is, then, implicitly coupled with the divergence-free constraint on the velocity, without the existence of a time dependence. Since these are the main differences from compressible flow calculation, this constraint implies that time integration of the incompressible flow equations is not possible in a straightforward manner.

Soh and Goodrich [26] cite the three main approaches for the solution of incompressible, inert Navier–Stokes equations and present a new approach based on the method developed by Chorin [3]. The proposed method consists in applying the Crank–Nicolson standard approximation for all linear and non-linear terms, including pressure and a pseudo-time which is introduced between two physical time steps. This procedure is used to solve the non-linear system for the divergence-free velocity field at the advanced time level. The continuity equation, preconditioned with a pseudo-time derivative of the pressure, and the momentum equations depend on both the physical and the pseudo-time derivatives. The steady state in pseudo-time is achieved efficiently because it does not require a divergence-free velocity field. The physical

solution at the advanced time level is obtained when the system of preconditioned equations in pseudo-time achieves the steady solution.

For steady reacting incompressible flows with heat release, Bruel *et al.* [4] have shown that the pseudo-compressibility technique has a high performance in terms of convergence and robustness. Based on this characteristic, Corvellec *et al.* [5, 6] add the physical time derivative of density to the preconditioned continuity equation proposed by Soh and Goodrich [26] in order to obtain a time accurate equation. Therefore, the time accurate, modified continuity equation can be written in the following generic form:

$$\frac{\partial \bar{\rho}}{\partial t} + \frac{1}{\beta}\frac{\partial \bar{p}}{\partial \tau} + \frac{\partial \bar{\rho}\tilde{u}_i}{\partial x_i} = 0 \tag{8}$$

where β is the pseudo-compressibility factor expressed in $m^2\,s^{-2}$, τ is the pseudo-time, t is the physical time and $\bar{p}$ is the static pressure. Equation (8) is written using the classical Favre [20] averaging procedure. In the present paper, the exact same approach is used, except that it is reinterpreted in a cell-vertex, hybrid unstructured grid, finite volume formulation.

Bruel *et al.* [4] show that, from the analysis carried out by Chang and Kwak [27], two pseudo-Mach numbers and pseudo-sound speeds should be considered: one for the reactants and another for the products. The pseudo-Mach number for the reactants, M_r, and for the products, M_b, are expressed as

$$M_r = \frac{u_r}{a_r}, \quad M_b = \frac{u_b}{a_b} \tag{9}$$

where u_r and u_b are the convection velocities, and a_r and a_b are the pseudo-sound speeds, with r and b subscripts indicating reactants and products, respectively. In generic form, the pseudo-sound speed is given by

$$a = \sqrt{u^2 + \beta} \tag{10}$$

More details about the analysis carried out for premixed reacting flow can be obtained from Bruel *et al.* [4], where the evolution of the quantity M_r/M_b, as a function of the reduced pseudo-compressibility factor $\hat{\beta} = \beta/u_r^2$, is discussed. In Section 7, a brief numerical sensitivity analysis of the present method to this dimensionless parameter is presented.

3. GOVERNING EQUATIONS

Despite the fact that the test cases presented here are characterised by one-dimensional mean properties, the governing equations are presented and solved in a two-dimensional form with the perspective that the proposed method will be used for the calculation of multi-dimensional flows in the future. For the BML model, the main variables that describe a reactive turbulent flow are the density, $\bar{\rho}$, the Cartesian velocity components, $\tilde{u}_i$, the static pressure $\bar{p}$ and the reaction progress variable $\tilde{c}$.

The distribution of these variables in the computational domain is obtained through the solution of the Navier–Stokes equations, with the continuity equation modified by the pseudo-compressibility approach as given by Equation (8), and a balance equation for the reaction progress variable. The momentum and progress variable equations are also modified to incorporate the unsteady terms related to the artificial compressibility approach, following in that

respect the technique of Rogers *et al.* [28, 29], Soh and Goodrich [26] and Corvellec *et al.* [5, 6]. Accordingly, a pseudo-time derivative is added to the time-dependent Navier–Stokes equations. These equations, together with the time accurate, preconditioned continuity equation (8), form the set of equations to be solved. Hence, using the classical Favre [20] average, the set of equations, written in a fixed system of co-ordinates and in a conservative vector form, is given by

$$\frac{\partial Q}{\partial t} + \frac{\partial q}{\partial \tau} + \frac{\partial E_{e_i}}{\partial x_i} - \frac{\partial E_{v_i}}{\partial x_i} = S \tag{11}$$

The equation of state is given by Equation (5) and the various terms which appear in Equation (11) are defined by

$$Q = \begin{Bmatrix} \bar{\rho} \\ \bar{\rho}\tilde{u} \\ \bar{\rho}\tilde{v} \\ \bar{\rho}\tilde{c} \end{Bmatrix}, \quad q = \begin{Bmatrix} \bar{p} \\ \bar{\rho}\tilde{u} \\ \bar{\rho}\tilde{v} \\ \bar{\rho}\tilde{c} \end{Bmatrix}, \quad E_{\mathrm{e}_x} = \begin{Bmatrix} \beta\bar{\rho}\tilde{u} \\ \bar{\rho}\tilde{u}^2 + \bar{p} \\ \bar{\rho}\tilde{u}\tilde{v} \\ \bar{\rho}\tilde{u}\tilde{c} \end{Bmatrix}, \quad E_{\mathrm{e}_y} = \begin{Bmatrix} \beta\bar{\rho}\tilde{v} \\ \bar{\rho}\tilde{u}\tilde{v} \\ \bar{\rho}\tilde{v}^2 + \bar{p} \\ \bar{\rho}\tilde{v}\tilde{c} \end{Bmatrix}$$

$$E_{\mathrm{v}_x} = \begin{Bmatrix} 0 \\ \bar{\sigma}_{xx} - \bar{\rho}\widetilde{u''u''} \\ \bar{\sigma}_{xy} - \bar{\rho}\widetilde{u''v''} \\ \bar{\rho}D\dfrac{\partial \tilde{c}}{\partial x} - \bar{\rho}\widetilde{u''c''} \end{Bmatrix}, \quad E_{\mathrm{v}_y} = \begin{Bmatrix} 0 \\ \bar{\sigma}_{xy} - \bar{\rho}\widetilde{u''v''} \\ \bar{\sigma}_{yy} - \bar{\rho}\widetilde{v''v''} \\ \bar{\rho}D\dfrac{\partial \tilde{c}}{\partial y} - \bar{\rho}\widetilde{u''c''} \end{Bmatrix}, \quad S = \begin{Bmatrix} 0 \\ 0 \\ 0 \\ \bar{w} \end{Bmatrix} \tag{12}$$

where $\bar{w}$ is the mean reaction rate given by Equation (7), and ϕ'' is the fluctuation of ϕ around $\tilde{\phi}$. The laminar stress tensor for a Newtonian fluid, σ_{ij}, is given by

$$\sigma_{ij} = \mu_l \left(\frac{\partial u_i}{\partial x_j} + \frac{\partial u_j}{\partial x_i} - \frac{2}{3}\frac{\partial u_k}{\partial x_k}\delta_{ij} \right) \tag{13}$$

In Equation (11), q is the preconditioned depending variable vector and Q the physical time depending variable vector. The x and y indexes refer to Cartesian components, E_{e} and E_{v} are, respectively, the Euler and Navier–Stokes flux vectors given in Equation (12) which, in the vectorial notation form, are written by $\mathbf{E} = E_x\hat{\imath} + E_y\hat{\jmath}$. As a short remark, the Navier–Stokes equations are written for Eulerian co-ordinates in the present work, whereas Corvellec [5] and Corvellec *et al.* [6] use a one-dimensional formulation with the reference frame attached to the flame.

The turbulent transport terms, that is the Reynolds stresses, present in Equation (12) need a closure. For the momentum equations, the Reynolds stress tensor is modelled using a Boussinesq-like formulation based on the turbulent viscosity concept (see Reference [30]):

$$\bar{\rho}\widetilde{u_i''u_j''} = -\mu_t \left(\frac{\partial \tilde{u}_i}{\partial x_j} + \frac{\partial \tilde{u}_j}{\partial x_i} \right) + \frac{2}{3}\left(\bar{\rho}\tilde{k} + \mu_t \frac{\partial \tilde{u}_k}{\partial x_k} \right)\delta_{ij} \tag{14}$$

where $\tilde{k} = \frac{1}{2}\widetilde{u_i''u_i''}$ is the kinetic turbulent energy equal to $\frac{3}{2}\widetilde{u''u''}$ for the homogeneous isotropic frozen turbulence considered here. With this type of gradient modelling for the Reynolds

stresses, a new unknown variable, μ_t, appears. This variable is the turbulent viscosity coefficient, which is not a property of the fluid as the molecular viscosity, but which depends on the flow characteristics varying in space and time. Launder and Spalding [31] showed by dimensional analysis that

$$\mu_t = \bar{\rho} C_\mu \frac{\tilde{k}^2}{\tilde{\varepsilon}} \tag{15}$$

with C_μ being an experimental constant equal to 0.09.

In the present work, the turbulent kinetic energy, $\tilde{k}$, and its dissipation rate, $\tilde{\varepsilon}$, are considered constant and equal to the values that prevail in the reactants. They are obtained through the prescription of the root mean square velocity fluctuations $u'_{\mathrm{r}} = \sqrt{\overline{u'^2_{\mathrm{r}}}}$ and the turbulence integral length scale l_i namely:

$$\tilde{k} = \tfrac{3}{2} u'^2_{\mathrm{r}}, \quad \tilde{\varepsilon} = C_\mu^{0.75} \frac{\tilde{k}^{3/2}}{l_i} \tag{16}$$

A gradient hypothesis is also adopted to close the turbulent scalar flux $\bar{\rho}\widetilde{u''c''}$, namely (see Reference [16]):

$$\bar{\rho}\widetilde{u''_i c''} = -\frac{\mu_t}{Sc_t} \frac{\partial \tilde{c}}{\partial x_i} \tag{17}$$

where Sc_t is the turbulent Schmidt number.

Equations (11), written in integral form using Green's theorem, are given by

$$\frac{\partial}{\partial t}\int_V Q \,\mathrm{d}V + \frac{\partial}{\partial \tau}\int_V q \,\mathrm{d}V + \oint_{\mathscr{S}} \mathbf{E}_{\mathrm{e}} \cdot \vec{\mathbf{n}} \,\mathrm{d}\mathscr{S} = \oint_{\mathscr{S}} \mathbf{E}_{\mathrm{v}} \cdot \vec{\mathbf{n}} \,\mathrm{d}\mathscr{S} + \int_V S \,\mathrm{d}V \tag{18}$$

where $\vec{\mathbf{n}}$ is the outgoing normal unit vector to surface $\mathscr{S}$ of volume V.

4. SPATIAL DISCRETIZATION

The physical time-dependent properties and the static pressure p are stored at the vertices of the elements. The control volume for a given vertex, i, is defined by all elements having i as a common vertex, as shown in Figure 1. As the control volume can be constructed by different types of elements on a hybrid grid topology (triangles and/or quadrilaterals), the elementary cell is named here an element. The boundary flux integral in Equation (18) is approximated, as usual in the finite-volume formulation, using the trapezoidal rule of integration, which can be shown to be equivalent to a piecewise linear Galerkin approximation with a lumped mass matrix (see References [32, 33]). Although better shock resolution and the capture of other discontinuities, as thin flames, can be obtained using some upwind-based methods (see References [34–38]), the present formulation is generally better suited for explicit schemes and it has lower computational cost. To overcome that drawback, a local adaptive refinement of the mesh should be used in critical areas of the flow field. The flux vectors, E_{e} and E_{v}, are computed at the vertices on the outer boundary of the control volume. This scheme is based on Mavriplis *et al.* [32, 33] and it proves to be a good technique for the solution of inert steady

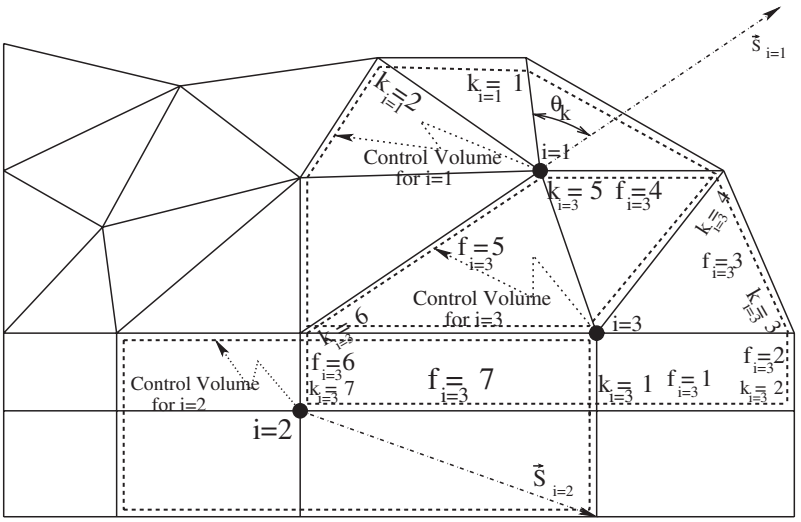

Figure 1. Domain of influence of nodes 1–3 and their local stretching vector $\vec{\mathbf{S}}$ for hybrid unstructured grid.

and unsteady flow, as presented by Dourado *et al.* [7–9], Marviplis and Venkatakrishnan [39] and Mavriplis [40]. A similar discretisation based on a finite elements approach is presented by Manzari *et al.* [41].

Thus, Equation (18) can be written in discretised form as

$$V\frac{\partial \bar{Q}_i}{\partial t}+V\frac{\partial \bar{q}_i}{\partial \tau}+\sum_{f=1}^{nf}(\bar{E}_{e_x f}\Delta y-\bar{E}_{e_y f}\Delta x)=\sum_{f=1}^{nf}(\bar{E}_{v_x f}\Delta y-\bar{E}_{v_y f}\Delta x)+V\bar{S} \tag{19}$$

where

$$\bar{q}=\frac{1}{V}\int_V q\,\mathrm{d}V,\quad \bar{Q}=\frac{1}{V}\int_V Q\,\mathrm{d}V \tag{20}$$

are the average-dependent variable vectors for pseudo-time τ and physical time t, respectively, and

$$\bar{S}=\frac{1}{V}\int_V S\,\mathrm{d}V \tag{21}$$

is the average source term vector. It is assumed that $Q=Q(q)$ with the help of the state equation given by Equation (5). In two-dimensional Cartesian co-ordinates, the product $\vec{\mathbf{n}}\,\mathrm{d}\mathscr{S}$ is given by

$$\vec{\mathbf{n}}\,\mathrm{d}\mathscr{S}=\Delta y\hat{\imath}-\Delta x\hat{\jmath} \tag{22}$$

As explained before, $\bar{E}$ is the average flux vector at face f calculated as the arithmetic average of the two fluxes located on the nodes that delimit this face. Here, $\hat{\imath}$ and $\hat{\jmath}$ are the unit vector

in the Cartesian space. Then, for a given face f, the flux vector associated to it is given by

$$\bar{E}_f = \frac{E_{n1,f} + E_{n2,f}}{2} \tag{23}$$

where $E_{n1,f}$ and $E_{n2,f}$ are the flux vectors at nodes $n1$ and $n2$ that delimit the considered face f. Further details for triangular and hybrid elements on an unstructured grid context are presented in previous works (see References [8, 9]).

The implemented algorithm has an edge-based data structure. On an overlapped hybrid grid finite volume context there are several configurations to calculate the flux balance of a given edge. For example, let us consider the face delimited by the nodes $(k=1)_{i=3}$ and $(i=3)$, represented in the Figure 1, named in this case nodes $n1$ and $n2$, respectively. In this way, the face direction is also defined. The mean flux vector, inviscid $\bar{E}_{\mathrm{e}f}$ as viscous $\bar{E}_{\mathrm{v}f}$, are calculated using Equation (23) and their products with Equation (22) give the respective inviscid and viscous fluxes through this face. For the element on the left side of this face, these fluxes are added into volumes for the nodes $(k=6)_{i=3}$ and $(k=7)_{i=3}$. And for the element on the right side, these fluxes are subtracted from the volumes associated with the nodes $(k=2)_{i=3}$ and $(k=3)_{i=3}$. If now the considered face is delimited by the nodes $(k=2)_{i=3}$ and $(i=3)$, the fluxes of this face are added in the balance of the volume for the node $(i=1)$ and subtracted from both volumes for the nodes $(i=2) \equiv (k=7)_{i=3}$ and $(k=1)_{i=3}$. Finally, for the face delimited by the nodes $(i=1)$ and $(k=4)_{i=3}$, the fluxes through these faces are computed only for the volumes for the nodes $(i=1)$ and $(k=3)_{i=3}$. It should be emphasized that the flux calculation procedure here described, using an overlapped hybrid grid, is an original contribution by the authors. Clearly, this procedure was inspired in previous works in the literature, but to the authors' knowledge, there have not been such an implementation before for an overlapped hybrid grid.

Barth and Jespersen [11] present a discussion about the gradient estimation for higher-order schemes, and suggest that two constraints must be satisfied. For a given property, Φ, the gradient estimation needs an exact calculation of $\nabla\Phi_i$ when Φ_i has a linear variation and $\nabla\Phi_i$ must be defined for arbitrary meshes. The gradient estimate should be accurate in order to keep at least the same order of accuracy of the convective terms. They appear in the stress tensor terms in Equations (13) and (14) and in the modelling of the turbulent mass flux term $\bar{\rho}\widetilde{u''c''}$, given by Equation (17). In this work, the gradients are computed, following Barth and Jespersen [11], by

$$\int_V \nabla\Phi \, \mathrm{d}V = \oint_{\mathscr{S}} \Phi \cdot \vec{\mathbf{n}} \, \mathrm{d}\mathscr{S} \tag{24}$$

The estimate of the gradient is given by computing the boundary integral (24)

$$\nabla\Phi = \frac{1}{V} \oint_{\mathbf{S}} \Phi \cdot \vec{\mathbf{n}} \, \mathrm{d}\mathbf{S} \tag{25}$$

As noted by Barth and Jespersen [11], in the cell vertex scheme, the gradients are calculated at the vertices on the outer boundary that delimit the control volume of a given node i (see Figure 1).

Thus, in a cell vertex context, the gradient discretisation has the final form given by

$$\nabla\Phi = \frac{1}{V}\sum_{f=1}^{nf}\left[\left(\frac{\vec{\mathbf{\Phi}}_{n1,f}+\vec{\mathbf{\Phi}}_{n2,f}}{2}\right)\cdot(\vec{\mathbf{n}}\,\mathrm{d}\mathscr{S})_f\right] \tag{26}$$

Using the definition given by Equation (22), this last equation can be written as

$$\nabla\Phi = \frac{1}{V}\sum_{f=1}^{nf}\left[\left(\frac{\vec{\mathbf{\Phi}}_{n1,f}+\vec{\mathbf{\Phi}}_{n2,f}}{2}\right)\cdot(\Delta y\hat{\imath}-\Delta x\hat{\jmath})_f\right] \tag{27}$$

Here the same approach of trapezoidal rule as used for the discretisation of the convective terms is adopted. It is easy to show that this approach is equivalent to a second-order finite difference on an homogeneous mesh. The sub-indexes $n1$ and $n2$ have the same meaning as given before. This procedure is equivalent to the procedure adopted by Mavriplis *et al.* [32]. Other methods to calculate the gradients to construct viscous or diffusive terms are proposed in the literature. However, the method used here has shown to be simple and robust enough for the proposed calculations. Additionally, the proposed discretisation of the gradients given by Equation (27) is easily adapted for arbitrary meshes, satisfying one of the constraints pointed by Barth and Jespersen [11].

5. ARTIFICIAL DISSIPATION

For high Reynolds number flows, the viscous terms of the Navier–Stokes equations become incapable of providing proper dissipation for stability. The use of highly refined grid throughout the domain may produce the necessary dissipation, but it results in significant increase in CPU time. Thus, additional artificial dissipation terms are needed to stabilise the method in the subsonic regime and reduce the need for more expensive highly refined grids. These additional dissipative terms cannot compete with physical dissipation in regions where the viscous phenomena are important and the accuracy of the scheme must be preserved in those regions of he flow field. Here, an appropriate fourth difference bi-harmonic dissipation term is added as suggested by Mavriplis *et al.* [32] and applied by Dourado *et al.* [9] along with a second difference term. A switch based on the pressure gradient is adopted to turn on and off the second difference artificial dissipation term with the correct value, depending on the flow local characteristics.

Thus, taking into account that the adopted artificial dissipation operator used here is a blend of an undivided Laplacian and a biharmonic operator, it can be written as

$$D_{\mathrm{a}}(q_i) = \sum_{k=1}^{nn}[\Delta_k - \Delta_i]\left[\frac{A_k + A_i}{2}\right] \tag{28}$$

where

$$\Delta(q) = k'^{(2)}q - k^{(4)}\nabla^2 q \tag{29}$$

and nn is the number of nodes located on the boundary of the control volume which delimits the volume i, as sketched in Figure 1. The A coefficients are added to adjust these terms for

highly stretched meshes and preserve the scheme accuracy in viscous dominated regions. The $k'^{(2)}$ coefficient is proportional to an undivided Laplacian of the pressure, which is constructed as the summation of the pressure differences along all edges defining the ith control volume. It is expressed as

$$k'^{(2)} = k^{(2)} \frac{\sum_{k=1}^{nn} |p_k - p_i|}{\sum_{k=1}^{nn} |p_k + p_i|} \tag{30}$$

The second-order term is important only in presence of high pressure gradients, such as found typically in shocks. Since the code used here is based on a compressible code, the authors decided to keep all the artificial dissipation terms. As a consequence, the $k^{(2)}$ constant has to be set to zero and an appropriated implementation was devised in order to save computational time avoiding wasted operations. The constant which defines the level of fourth order dissipation $k^{(4)}$ is equal to $1/256$ for all calculations presented in this work. This value has been adequate and ideal for both compressible and incompressible schemes, giving stability, good convergence and practically no influence on the physical terms of the discretised governing equations. In Section 7 a short study about the effect of $k^{(4)}$ on convergence and pressure gradients versus the progress reaction variable $\tilde{c}$ will be presented.

As discussed by Mavriplis *et al.* [32], the A coefficient must take into account both the spectral radius and the aspect ratio of the considered control volume on a stretched mesh. Then, it is necessary to adjust the correct level of this dissipation term on highly stretched regions and to avoid the competition of this artificial dissipation term with the physical one. This is done by taking:

$$A_k = \alpha_{1k} \cos^2 \theta_k + \alpha_{2k} \sin^2 \theta_k \tag{31}$$

with subscript i and k corresponding to the variable evaluated at nodes i and k, respectively. The expressions of the coefficients α_1 and α_2 in Equation (31) are based on the isotropic value of the maximum eigenvalue λ at each point of the mesh

$$\alpha_1 = \phi(s) \frac{1}{s+1} \lambda, \quad \alpha_2 = \phi(s^{-1}) \frac{s}{s+1} \lambda \tag{32}$$

where s represents the magnitude of the stretching vector $\vec{\mathbf{S}}$ (see Figure 1) and $\phi(r) = 1 + r^{2/3}$. For unstructured meshes, an isotropic value of the maximum eigenvalue λ of the Euler equations at each mesh point is given in a discrete approximation by

$$\lambda = \sum_{f=1}^{nf} |\bar{u}_f \Delta y_f - \bar{v}_f \Delta x_f| + \bar{a}_f \sqrt{\Delta x^2 + \Delta y^2} \tag{33}$$

with $\bar{u}$ and $\bar{v}$ are the Cartesian velocity components and $\bar{a}$ is the speed of sound that takes into account the pseudo-sound speed given by Equation (10). These properties are given by the average of the properties from the two nodes that delimits the face f, over all boundary faces nf of the considered volume. As the code is edge-base organised, this artificial dissipation term

was enhanced in order to be consistent with the hybrid grid, where triangular and quadrilateral elements coexist, in order to keep the conservative characteristic of the scheme. Two imaginary diagonals are created in quadrilateral elements connecting the opposite nodes. Those imaginary diagonals must also be taken into account in the process of selecting the stretching vector $\vec{\mathbf{S}}$ of a control volume (see Figure 1). Such an enhancement in the construction of the artificial dissipation terms for a hybrid grid is also an original contribution of the present work. The projection strategy for the volumes situated over a wall type boundary is taken from Mavriplis [33]. This strategy is adopted to avoid a false normal gradient due to the way the Laplacian is numerically evaluated. In this work, the projection strategy was appropriately adapted for hybrid grids to take into account both triangular and quadrilateral elements on the boundary.

6. PSEUDO AND PHYSICAL-TIME MARCHING

As explained in the previous section, in this work a time accurate unsteady solution consisting of a steady solution on a pseudo-time for each physical time step is sought. The pseudo-compressibility method is based on the solution of the time-dependent Navier–Stokes and progress variable balance equations written in a conservative form. In order to find the steady solution during each physical time step, it is necessary to solve the discretised linear system of Equation (19). Thus, the physical time derivative is treated as a source term and written in a form similar to that presented in Equation (21), such that

$$\bar{S}_T = \frac{1}{V}\int_V \frac{\partial Q}{\partial t}\,\mathrm{d}V \tag{34}$$

where $\bar{S}_T$ is the physical time source term. The time discretisation of this term will be discussed later in this section. This set of coupled equations can by written as

$$V_i \frac{\mathrm{d}q_i}{\mathrm{d}\tau} + [C(q_i) - D_{\mathrm{v}}(q_i) - D_{\mathrm{a}}(q_i)] = S(q_i) - S_T(q_i), \quad i = 1 \ldots n \tag{35}$$

In the equation above, $C(q)$ is the residual of the convective inviscid term, $D_{\mathrm{v}}(q)$ represents the viscous dissipation term and $D_{\mathrm{a}}(q)$ is the artificial dissipation. The source terms related to the reactive Navier–Stokes equations are represented by $S(q)$, and $S_T(q)$ is the physical time related source term.

Although implicit schemes improve considerably the efficiency of the time integration necessary to obtain the steady solution, these schemes are not trivial to implement in an unstructured grid context. Thus the authors decided to adopt an explicit scheme to calculate both steady and unsteady reacting flows with heat release. Explicit schemes are easy to implement both in sequential and in parallel architectures, which is envisaged for future work. In the present work, an explicit three-stage hybrid Runge–Kutta time-stepping scheme was adopted for time integration of pseudo-time due to its simplicity, robustness and low computational cost. The resulting scheme has a satisfactory performance and good efficiency on unstructured grid algorithm. The scheme to advance the solution on pseudo-time step proposed by

Manzari *et al.* [41] is here implemented in the form:

$$\begin{aligned} q_i^{(0)} &= q_i^n \\ q_i^{\kappa} &= q_i^{(0)} - \alpha_\kappa \frac{\Delta\tau}{V_i}[C(q_i^{(\kappa-1)}) - D_{\mathrm{v}}(q_i^{(\kappa-1)}) \\ &\quad -S(q_i^{(\kappa-1)}) + S_T(q_i^{(\kappa-1)}) - D_{\mathrm{a}}(q_i^{(0)})] \quad \text{for } \kappa = 1,2,3 \\ q_i^{n+1} &= q_i^{(3)} \end{aligned} \tag{36}$$

Here the operators C, D_{v} and S are created using the properties vector $q_i^{(\kappa-1)}$ from stage $\kappa-1$, while the artificial dissipation term is calculated only in the first stage and held constant throughout the next stages. The coefficients adopted in the Equation (36) are: $\alpha_1 = 0.6$, $\alpha_2 = 0.6$ and $\alpha_3 = 1.0$. The physical time derivative in Equation (34) is discretized by an second-order implicit Euler scheme given by

$$\left.\frac{\partial Q}{\partial t}\right|^{n+1,\kappa-1} = \frac{3Q^{n+1,\kappa-1} - 4Q^n - Q^{n-1}}{2\Delta t} \tag{37}$$

This time discretisation (Equation (37)) is adopted both by Rogers and Kwak [28] and Corvellec *et al.* [6] on a pseudo-time marching implicit scheme context. In the present work, it was adapted in order to be used with the pseudo-time marching explicit scheme given by Equation (36).

7. RESULTS

The test cases adopted to evaluate the proposed method consist of steady and unsteady planar premixed flames propagating freely. For unsteady flow calculations, the reactants are at rest and the flame propagates throughout the domain. In the steady flow calculations, the boundary conditions are imposed such that the flame does not move and the physical time derivatives are not considered. Consequently, the corresponding source term in Equation (35) vanishes. In the present work, the cases named by Corvellec [5] as Cases I and II are considered as test cases. The parameters of these slow and fast propagating flames are given in Table I.

The computational domain consists of a strip 0.5 m long and 0.1 m wide. The majority of the calculations performed in the present work adopt meshes constructed only by quadrilateral elements and only one division in the normal direction. This mesh topology is used because the stronger gradients occur in the longitudinal direction and the quadrilateral elements lead to the optimum discretisation (less number of elements for the same quantity of nodes) in

Table I. Parameters defining the test case.

Case	χ	$\chi c^\star$	S_{l_0} (m s^{-1})	$\tilde{u}_{\mathrm{r}}$ (m s^{-1})	$\widetilde{u_{\mathrm{r}}''}$ (m s^{-1})	l_i (m)	Sc_t	C_w (kg m^{-3} s^{-1})	$\bar{\rho}_{\mathrm{r}}$ (kg m^{-3})
I	5	0.03958	0.5	0.5	1.0	0.001	0.75	200	1.1886
II	5	0.03958	10.0	10.0	10.0	0.001	0.75	8000	1.1886

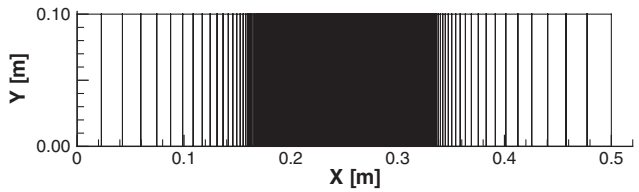

Figure 2. Computational mesh with 710 nodes and 354 quadrilateral elements named here as mesh 1.

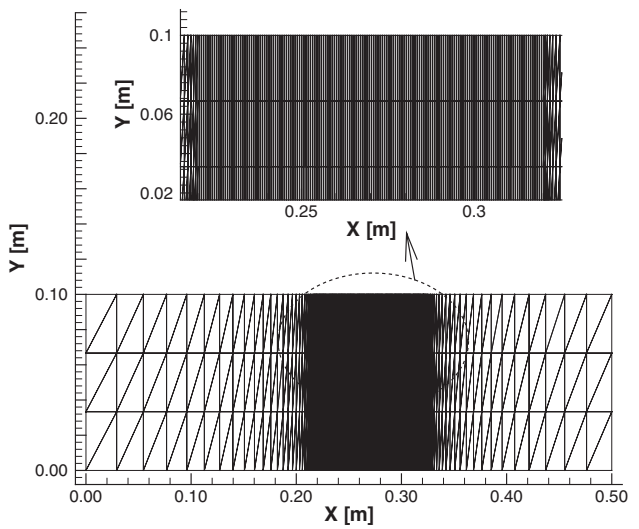

Figure 3. Computational mesh with 980 nodes composed by 561 quadrilateral elements and 342 triangular elements, named here as hybrid-mesh 1.

the normal direction. For highly stretched elements, such as those in more refined zones, very small angles between the faces of the elements and the direction of flow may lead to inaccurate flux calculation in Equation (19). A discussion about the effect of the shape of the elements is also presented in References [8, 9, 39]. The coarser mesh with only one division in the normal direction is shown in Figure 2 with 354 divisions in the longitudinal direction having a total of 710 nodes and 354 quadrilateral elements. Some different options for grid points distribution and topology in the longitudinal direction and their influence in the accuracy of the scheme will be presented later. Also, results using both triangular and quadrilateral elements are presented to show the capability of the proposed method to treat hybrid grids. An example of a hybrid grid used in this work with triangular and quadrilateral elements is shown in Figure 3.

The considered flow has a high Reynolds number with a constant turbulent viscosity μ_t, throughout the domain. As the laminar viscosity in Equation (13) is small compared with its turbulent equivalent, it is set to zero, $\mu_l = 0$. In a similar way, the laminar diffusion coefficient D in the balance equation of the reaction progress variable $\tilde{c}$ is considered equal to zero and therefore only the turbulent coefficient D_t is taken into account.

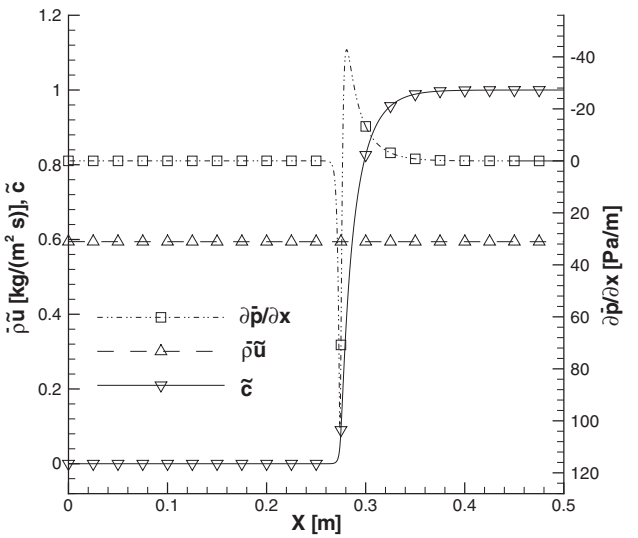

Figure 4. Profiles of mean reaction progress variable, mass flow per unit area ($\bar{\rho}\tilde{u}$) and pressure gradient along x direction for mesh 1 with $\beta = 75$ ($\mathrm{m^2\,s^{-2}}$).

Two boundary conditions are adopted to appropriately evaluate the proposed method for the simulation of steady and unsteady flows. For steady flow calculations, the incoming reactants velocity is imposed equal to the turbulent flame speed, $\tilde{u}_\mathrm{r} = S_{t_0}$, at the left side of the domain. Therefore, the flame front stays stationary on a fixed frame of reference. The rms velocity u'_r and the progress variable $\tilde{c} = 0$ are also imposed at the inlet. The pressure at this boundary comes from the calculations. On the other hand, for unsteady calculations, the boundary condition corresponds to a fresh mixture at rest, $\tilde{u}_\mathrm{r} = 0$, as will be better explained later. At the boundaries $Y = 0$ and 0.1 symmetry boundary condition are applied. This condition corresponds to imposing normal velocity and normal gradients to these boundaries equal to zero. At the outlet boundary, on the right side of the domain, only the pressure is imposed and all other variables come from the calculations.

For steady calculations, the ignition is given by the initial condition for the progress variable $\tilde{c}$ as a ramp function that goes from $\tilde{c} = 0$ at $x = 0.27\,\mathrm{m}$ to $\tilde{c} = 1$ at $x = 0.32\,\mathrm{m}$. The continuity equation in this cases gives the value of the product $\bar{\rho}\tilde{u}$ such that $(\bar{\rho}\tilde{u})_\mathrm{r} = (\bar{\rho}\tilde{u})_\mathrm{b} = \text{constant}$. The initial distribution of $\tilde{u}$ can be obtained from this form of the continuity equation, with $\tilde{c}$ given by the profile of ignition and $\bar{\rho}$ given by state equation (4). For all the present calculations, the numerical parameters for the artificial dissipation terms given by Equations (29) and (30) are $k^{(4)} = 1/256$ and $k^{(2)} = 0$. A short analysis of the influence of the fourth-order constant $k^{(4)}$ in the convergence rate and quality of the results will be presented. It will show that this value is a good compromise between convergence rate and a minimum influence on the results. This is also verified by other authors for inert compressible flows (see References [32, 33]).

The first results for steady flow obtained with the proposed method using mesh 1 are presented in Figure 4. It shows the variation of the pressure gradient ($\partial\bar{p}/\partial x$), progress variable $\tilde{c}$ and the mass flux per area unit $\bar{\rho}\tilde{u}$. The figure shows that the distribution of $\bar{\rho}\tilde{u}$ is indeed solenoidal.

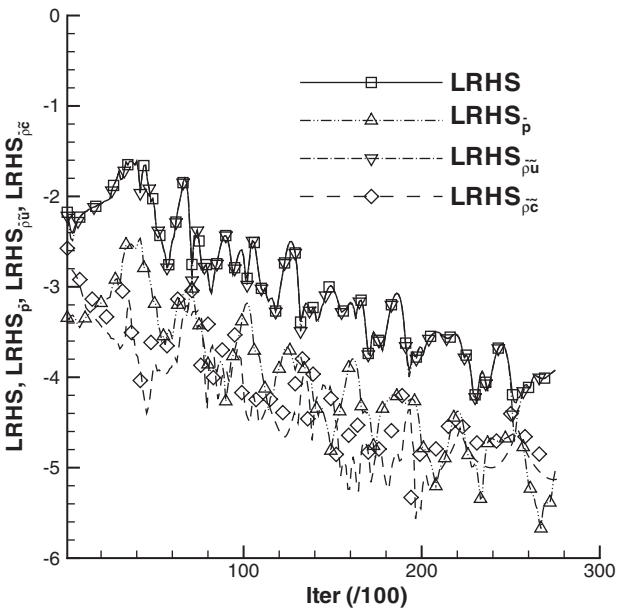

Figure 5. Convergence history of residual using mesh 1 with $\beta = 75$ ($m^2\ s^{-2}$).

No automatic adaptive grid technique was applied in the present work; therefore, the mesh needs to be refined near to the quench point $c^\star$, where the largest gradients appear. During the pseudo-time marching process the position where the strongest gradients appear may move forward or backward in the flow field until it reaches a steady state, when no more displacements occur. Hence, in order to keep the critical point in a region sufficiently refined during the pseudo-time marching, the computational grid has a uniformly spaced grid distribution along a path of domain. For mesh 1 shown Figure 2, this region with uniformly spaced nodes in the longitudinal direction is located between $0.17 \leqslant x \leqslant 0.33$ with 300 divisions. As a consequence, the minimum mesh spacing is $\Delta x_{\min} = 5.333 \times 10^{-4}$ m. A constant Courant–Friedrichs–Lewis (CFL) number equal to 0.94 is used throughout the domain for the steady flow. Thus, the pseudo-time step $\Delta\tau$ becomes variable and the minimum value is achieved in the finest region of the computational grid. The CFL number for the pseudo-time step is given by

$$\mathrm{CFL}_\tau = \lambda_\mathrm{b} \frac{\Delta\tau}{\Delta x_{\min}} \tag{38}$$

where $\lambda_\mathrm{b} = \tilde{u}_\mathrm{b} + \tilde{a}_\mathrm{b}$ is the greatest convective eigenvalue based on the pseudo-sound speed given by Equation (10). As a consequence, the minimum pseudo-time step for mesh 1 is equal to 2×10^{-5} s. The convergence for this test was achieved after 27 500 iterations as shown in the convergence history presented in Figure 5.

The profile of the pressure gradients versus the progress reaction variable, c, obtained with the present method for this first calculation is compared with the result presented by Corvellec [5]. The comparison is shown in Figure 6. It is possible to see good agreement between the

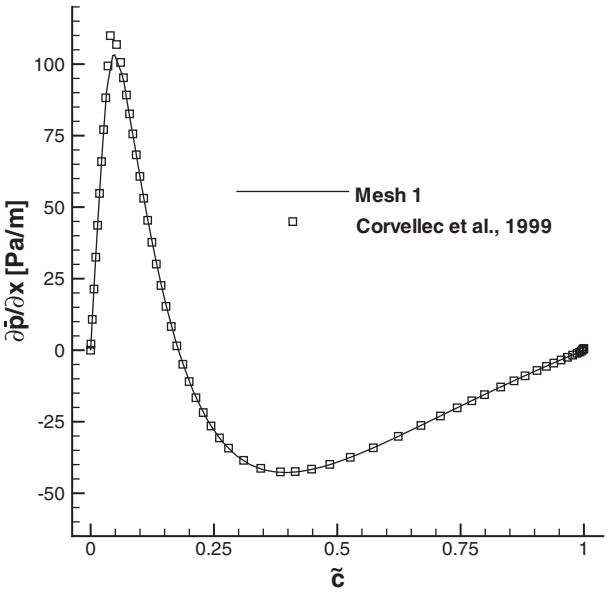

Figure 6. Profile of pressure gradient versus mean reaction progress variable for the mesh 1 with $\beta = 75$ ($m^{-2}\,s^{-2}$).

present calculation and the results obtained by Corvellec [5], with a slight difference in the maximum gradient. The maximum value of pressure gradient obtained with the present method using mesh 1 is 103.19 Pa m^{-1}, while Corvellec [5] obtained 110.28 Pa m^{-1}, resulting in a difference of 6%.

To analyse the effect of mesh refinement, three other space discretisations were adopted. The second, named mesh 2, has 50% more divisions in the x direction in the interval located between $0.17\,m \leqslant x \leqslant 0.33\,m$, giving $\Delta x_{min} = 3.56 \times 10^{-4}$ m. The third one, mesh 3, has 100% more divisions than mesh 1 in the same interval, which gives $\Delta x_{min} = 2.67 \times 10^{-4}$ m. The fourth mesh, named mesh 4, has the range of greater refinement reduced to $0.22\,m \leqslant x \leqslant 0.30\,m$, with the same quantity of nodes as mesh 3, which gives a minimum mesh spacing of $\Delta x_{min} = 1.33 \times 10^{-4}$ m. The final grid from Corvellec's who used auto-adaptative refinement has $\Delta x_{min,\,Corvellec} = 7.1 \times 10^{-5}$ m. The results obtained with all the meshes are presented in Figure 7, where the profiles of pressure gradients are plotted versus the mean reaction progress variable. In this figure it is possible to see the good agreement between the results obtained with the proposed method and the 1D method presented by Corvellec [5] on a structured mesh context. For the finest mesh, no difference between the results calculated here and the one presented in Reference [5] were observed. These results show that the proposed method is able to correctly capture the evolution of the pressure gradient throughout the flame.

A short analysis of the influence of the choice of the pseudo-compressibility factor β and the reduced pseudo-compressibility factor $\hat{\beta}$ on the convergence rate was carried out. Figure 8 presents the convergence history of x-direction momentum equation for several $\hat{\beta}$, using mesh 1. The results show that the residue of this equation is a good choice for convergence

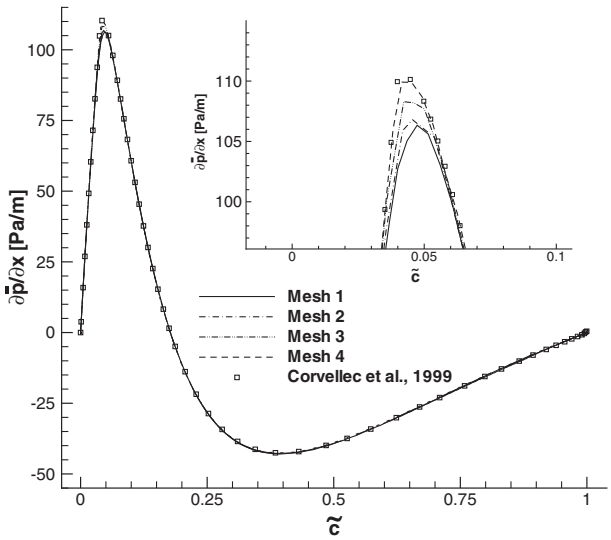

Figure 7. Profile of pressure gradient versus mean reaction progress variable for the meshes 1–4.

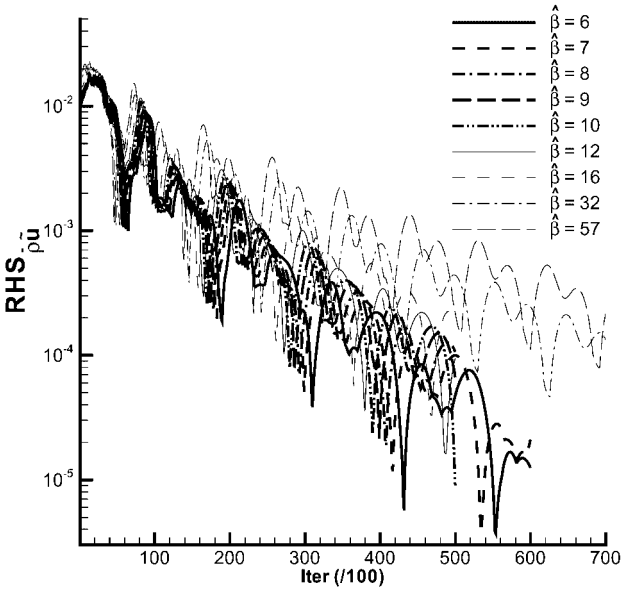

Figure 8. Error history for the x-direction momentum equation for several reduced pseudo-compressibility factor $\hat{\beta}$ using mesh 1.

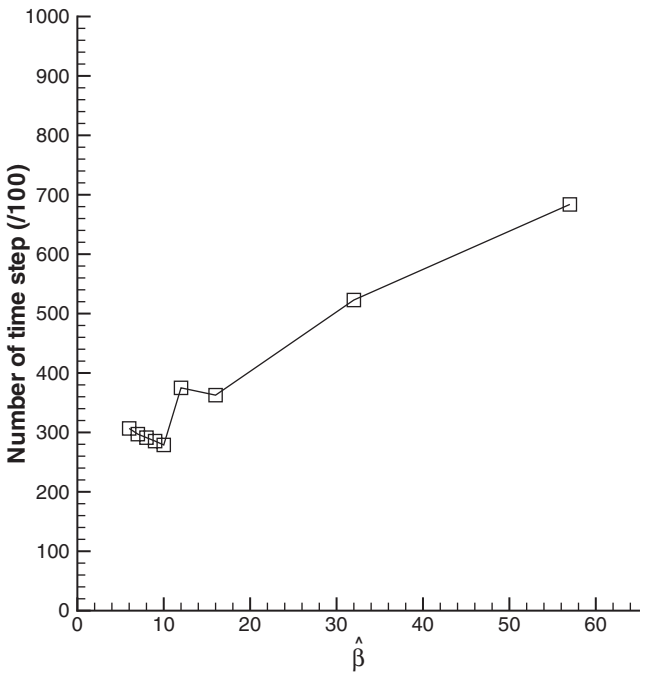

Figure 9. Number of time step necessary to achieve a converged solution ($\mathrm{LRHS}_{\tilde{\rho}\,\tilde{u}} \leqslant 10^{-4}\,\mathrm{kg\,m^{-2}\,s^{-2}}$).

criterion. Figure 9 shows the influence of reduced pseudo-compressibility factor $\hat{\beta}$ on the number of time steps necessary to achieve convergence. This result is obtained considering the convergence criteria for the referred equation as $\mathrm{LRHS}_{\tilde{\rho}\,\tilde{u}} \leqslant 10^{-4}$. The comparison between the results obtained by one of the authors (see Reference [4]) and the present results shows the same tendency for the optimum value of $\hat{\beta}$. It shows that the definition of pseudo-sound speed given by Equation (10) and the pseudo Mach number present by Bruel *et al.* [4] is also valid for the present 2D cell-vertex finite volume method. The results presented here have an optimum value of $\hat{\beta}_{\mathrm{opt}} \approx 8$, in agreement with Bruel *et al.* [4]. With the help of Figure 8 it is possible to verify that for very high values of the pseudo-compressibility factor the accuracy of the solution degrades.

Another short analysis carried out in this work considers the influence of the fourth-order dissipation term constant $K^{(4)}$ on the convergence rate and accuracy in the final solution. This analysis considers only the steady-state solution when the physical derivatives vanish. The calculation in this analysis used the grid named mesh 3, which is considered refined enough to produce good quality results and also save computational time. Another reason to adopt this grid is the fact that the main interest is in the effect of the level of artificial dissipation on the convergence and solution quality. The maximum root mean square of total residue is

$$\mathrm{RMS(RHS)} = \sqrt{\sum_{j=1}^{N_{\mathrm{eq}}} \max(\mathrm{RHS}_j)^2} \tag{39}$$

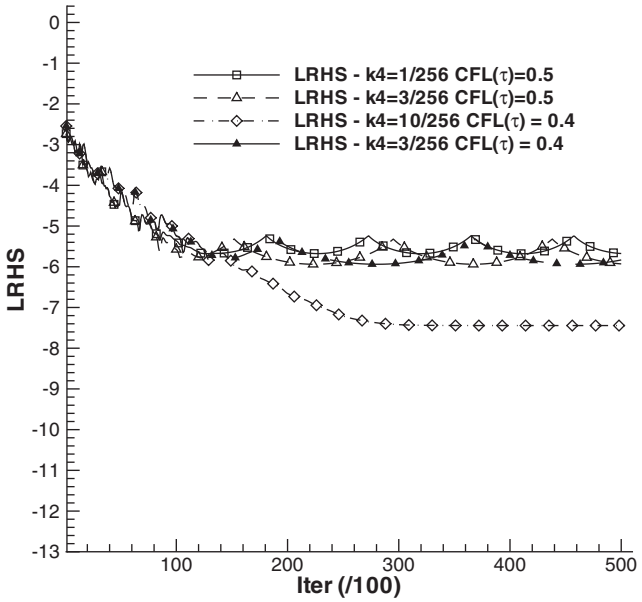

Figure 10. Error history for several fourth-order dissipation terms constant $K^{(4)}$ using mesh 3.

with N_{eq} the number of equations per volume, here is equal to 5. The max RHS_j is the maximum residue of equation j throughout the discretised domain. Figure 10 presents the historical evolution of the maximum root mean square of total residue of pseudo-time RMS(RHS). Based on the Figure 10 it is possible to verify that the calculation converges with approximately 15 000 iterations for all three values considered and that the largest value of $K^{(4)}$ leads to the lowest value of the residue. This behaviour is to be expected since the artificial dissipation terms are responsible for damping high-frequency error modes, created by the frequency cascading process in any non-linear formulation, which are beyond the resolution of the current mesh. Therefore, higher values of $K^{(4)}$ yield further damping and, hence, allow for further convergence of the solution. The influence of $K^{(4)}$ on the pressure gradient distribution through the flame is shown in the Figure 11. In general no perceived influence on the results is observed. However, it is possible to verify that the high gradients which exist in the region of discontinuity are more affected by a larger $K^{(4)}$. Then, a lower value of $K^{(4)}$ is preferable because it produces a minimum influence of the artificial dissipation on the physics of the phenomena, leading to a satisfactory convergence rate and ensuring numerical stability.

To evaluate the ability of the proposed method to calculate unsteady flows, a flame propagation throughout a fluid at rest is considered as test case. An initial profile of the flame front in a ramp is supplied as in the steady flow calculations presented before, and it propagates until it reaches a steady movement. This is similar to the unsteady numerical study performed by Corvellec [5]. Thus, to take into account the physical time-dependent phenomena, the related source term S_T indicated in the Equation (34) is calculated for each time step using the time discretisation presented in Equation (37). To obtain the new properties in the physical time t, the pseudo-time-depending equations are integrated by the Runge–Kutta scheme presented

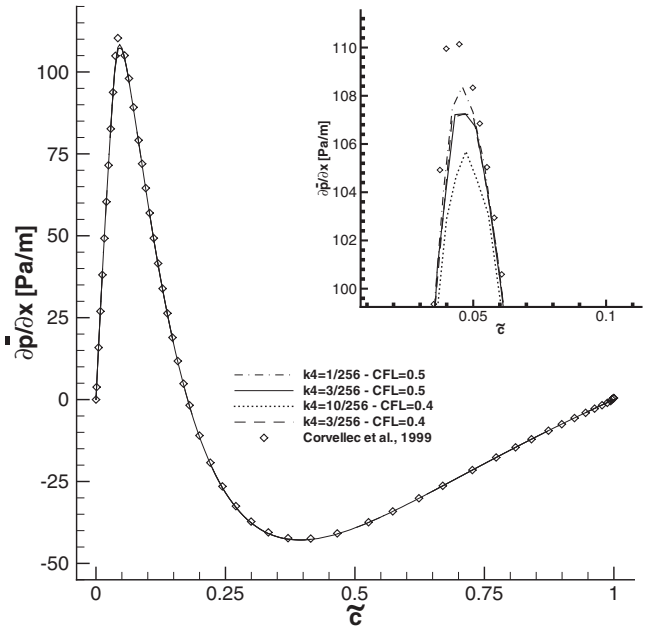

Figure 11. Fourth-order dissipation terms constant $K^{(4)}$ influence in the pressure gradient distribution.

in Equation (36) up to a defined convergence value or a limit of iterations. From the convergence analysis of steady-flow equations ($S_T = 0$) presented before, it was possible to define a convergence criteria to stop the pseudo-time integration. Thus, the adopted values for the residual of the momentum equation in x Cartesian direction is $\mathrm{RHS}(\bar{\rho}\tilde{u}) \leqslant 10^{-4.5}$ kg m^{-2} s^{-2}. The maximum number of iterations $\mathrm{NITER}(\tau)_{\max} \leqslant 20\,000$ is taken as adequate.

The physical properties are indicated in Table I. The flame brush, at $t = 0$, is supposed to be formed by the linear $\tilde{c}$ profile supposed to propagate at the flame speed S_{t_0} equal to the theoretical value obtained by Corvellec [5]. Accordingly, since the reactants are at rest, the incoming velocity imposed at the left side of the domain is null ($\overline{u_\mathrm{r}} = \tilde{u}_\mathrm{r} = 0$) and only the rms fluctuation u'_r is given. Eventually, the $\tilde{u}$ profile is initialised by the aid of the continuity equation and the equation of state as

$$\tilde{u} = \chi \tilde{c} S_{t_0} \tag{40}$$

The profiles of mean velocity $\tilde{u}$, the progress variable $\tilde{c}$, the static pressure $\bar{p}$ and the gradient $\partial \bar{p}/\partial x$ of the static pressure in the longitudinal direction are shown in Figure 12, at a given time after the flame front has reached a steady regime of propagation. It is also possible to see that the mass flow through the mean flame rush calculated by the present numerical method is equal to the theoretical value given by the steady equation (see Reference [5])

$$\rho_\mathrm{b} \bar{u}_\mathrm{b} = \frac{\rho_\mathrm{r}}{1+\chi} \chi S_{t0} = 0.495 \text{ kg m}^{-2} \text{ s}^{-1} \tag{41}$$

with the parameters of the Case I given in Table I. Figure 13 presents the profile of the pressure gradient $\partial \bar{p}/\partial x$ as a function of the progress variable $\tilde{c}$. As can be observed, the

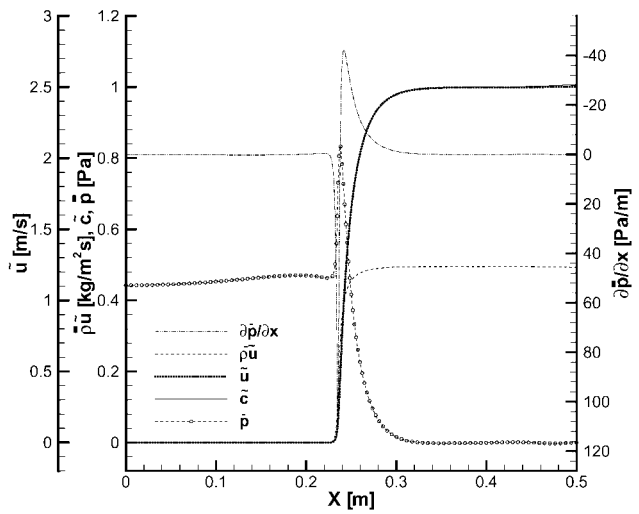

Figure 12. Several property profiles for unsteady flow using mesh 3.

same values are obtained with both steady and unsteady calculations. Figure 13 shows that the maximum value of $\partial \bar{p}/\partial x$ calculated with the present method using the mesh named mesh 3 coincides with the results obtained by Corvellec [5].

Figure 14 shows several progress variable profiles for different physical times, with a time step of 0.003 s. This figure leads to the conclusion that the steady propagation occurs after some delay of time and continues in a steady way afterwards. Based on Figure 15, it is possible to see that the front achieves the steady profile shape after approximately 0.022 s. This behaviour is similar to the results obtained by Corvellec [5] with an implicit one-dimensional approach.

In Figure 16, it is possible to see the evolution of the mean flame front speed. It shows that the present explicit two-dimensional method using an unstructured mesh technique predicts the same mean flame front speed S_t as the one-dimensional implicit method described in Reference [5], and tends asymptotically to the theoretical flame speed velocity S_{t_0}. The present method also shows good agreement with the analytical results available in Reference [5].

Finally, to test the robustness of the present method to calculate steady fast flame propagation, another test case was chosen, called case II. The properties for this test case are given in Table I. The profiles of the pressure gradient, the progress variable and the mass flux per unit area $\bar{\rho}\tilde{u}$ are presented in Figure 17. The variation of the progress reaction variable $\tilde{c}$ along the longitudinal co-ordinate x for both cases I and II calculated using the proposed numerical method is compared with the numerical results obtained by Corvellec [5] and presented in Figure 18. The profile of the pressure gradient distribution as a function of the progress reaction variable is given in Figure 19. The good agreement with the results of [5] obtained with an implicit method demonstrates that the present method is robust enough to capture correctly the pressure gradients for the fast flame. However, and as expected, the strong gradients observed for the fast flame flow requires the finest grid to be accurately resolved.

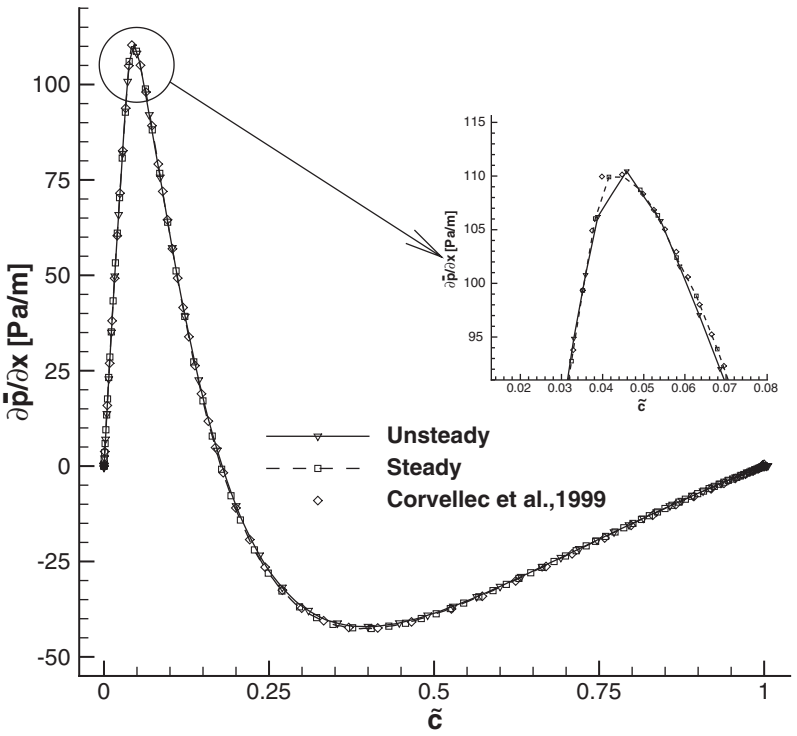

Figure 13. Profile of pressure gradient versus mean reaction progress variable for mesh 3 on unsteady calculation.

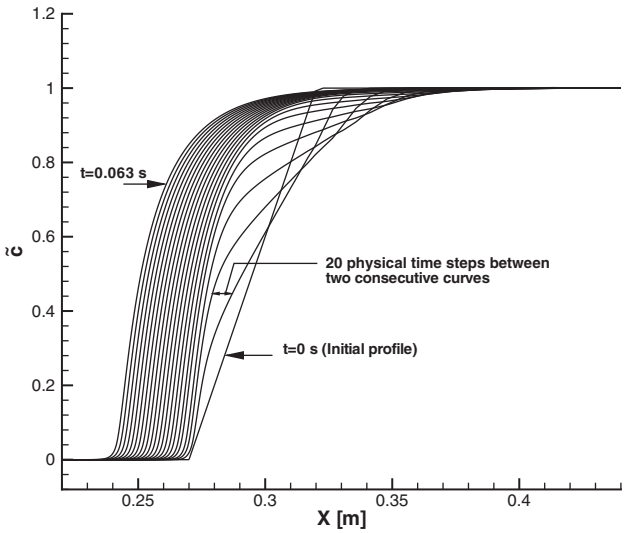

Figure 14. Flame front evolution for unsteady flow using mesh 3.

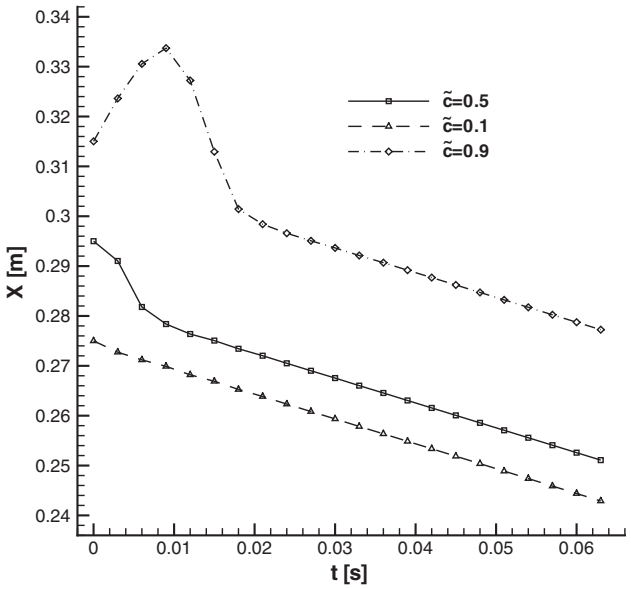

Figure 15. Time evolution of flame front for $\tilde{c} = 0.1$, $\tilde{c} = 0.5$ and $\tilde{c} = 0.9$.

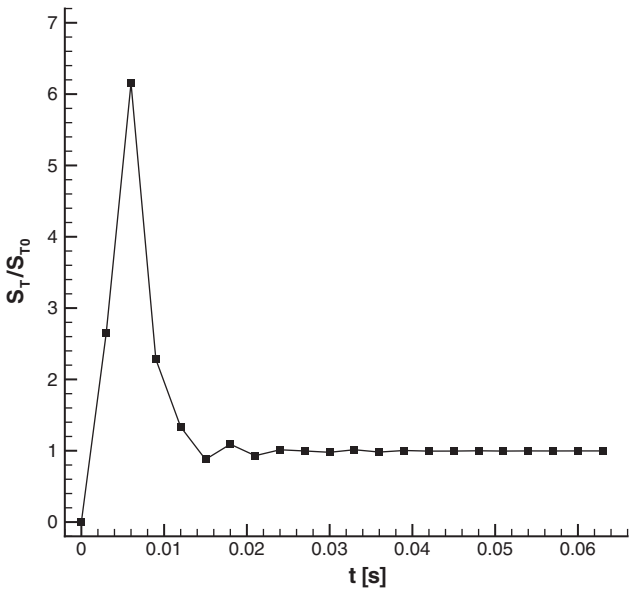

Figure 16. Mean flame front speed evolution for unsteady flow.

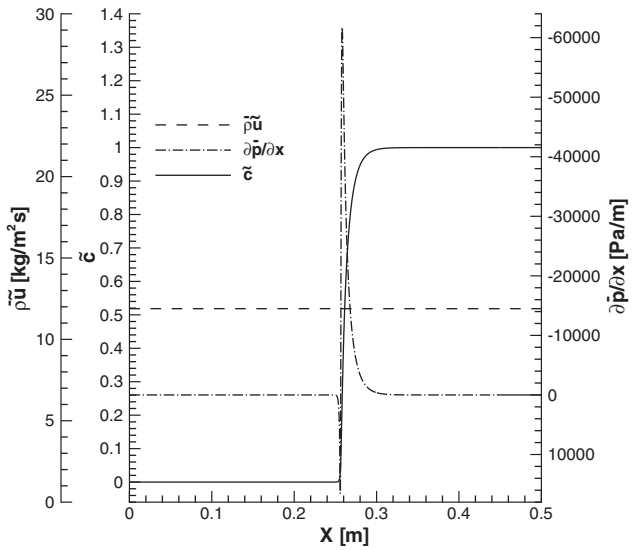

Figure 17. Profile of pressure gradient, progress variable and mass flow per unit area $\bar{\rho}\tilde{u}$ along x co-ordinate axis.

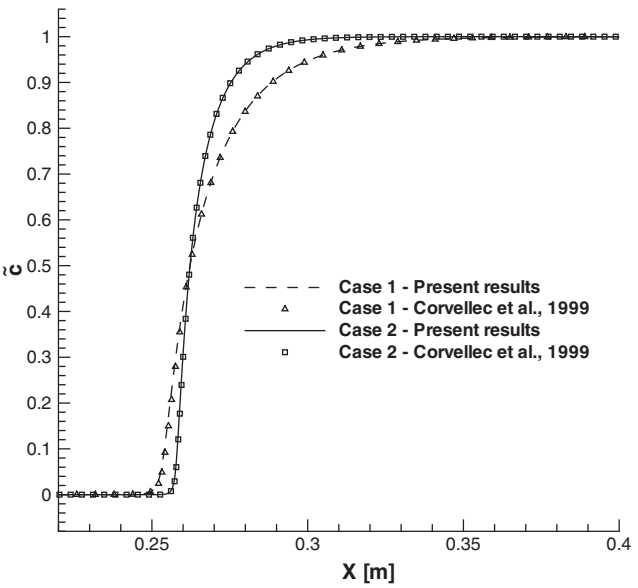

Figure 18. Mean flame front speed evolution for steady flow.

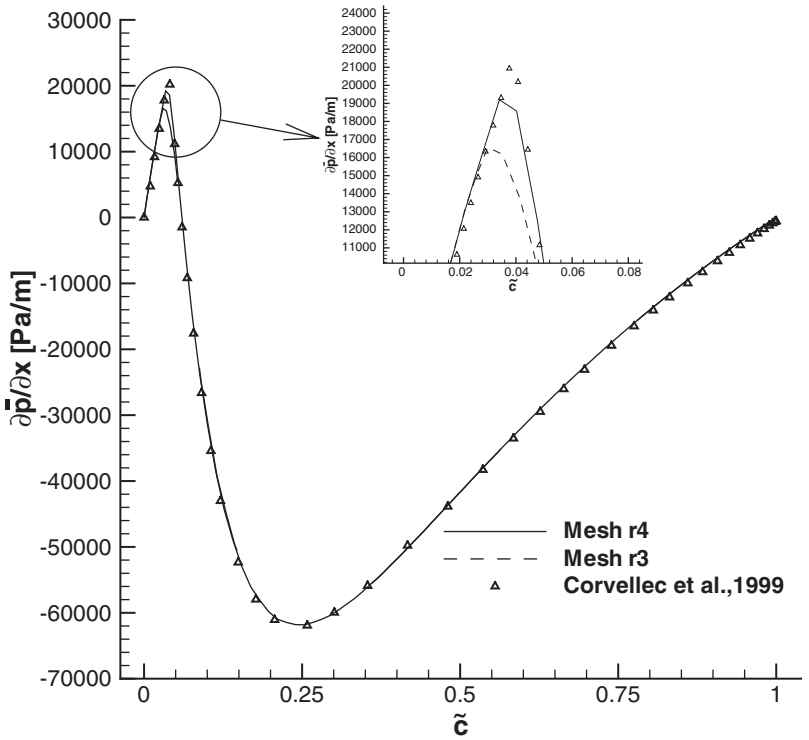

Figure 19. Profile of pressure gradient versus mean reaction progress variable for fast flame propagation—Case 2.

8. CONCLUDING REMARKS

With the results discussed in the present work, it is possible to draw the conclusion that the proposed scheme, based on the pseudo-compressibility method, applied to overlapped, cell vertex, finite volumes for hybrid grids, despite its simplicity, is a valid method to solve the governing equations for a reactive flow with premixed reactants in the limit of a zero Mach number. The solution of these equations by the proposed scheme gives results that are in good agreement with the analytical and numerical solutions available in the literature. The artificial dissipation terms included to stabilise the discretised governing equations and to avoid oscillations in the results do not influence the accuracy of the final solution. The artificial dissipation level is explicitly controlled by imposing the value of the $k^{(4)}$ constant.

As the adopted spatial discretisation uses co-located variables and since no upwind or vector flux splitting techniques are applied on the computation of convective flux terms, the code is simpler yet without loss of quality in the solutions. The comparison between the minimum grid interval obtained with the auto-adaptive 1D method, proposed by Corvellec *et al.* [5, 6], and the present method shows that, to achieve the same solution accuracy, the present scheme needs a coarser grid than that required by 1D method. Additionally, the use of an explicit, three-stage, hybrid, time stepping scheme has shown to be powerful enough to calculate the

steady solution in the pseudo-time for the discretised governing equations. The use of an explicit time stepping scheme has as drawback a lower maximum allowable CFL number, resulting in an increased total number of pseudo-time stepping iterations. On the other hand, the implementation is easier and each iteration is faster. Little effort is expected to be spent for a future code parallelisation, which can be the subject of future studies. Furthermore, the discretisation of the physical temporal derivative by an implicit scheme allows the recovery of the actual physical transients.

In conclusion, the proposed unstructured finite volume discretisation applied to the governing equations using the pseudo-compressibility method together with a physical time derivative can be used to calculate steady and unsteady combustion problems. Highly refined grids necessary to capture discontinuities require adaptive refinement techniques to become more competitive in practical industrial applications. In unsteady reactive flow cases, the flame brush may travel throughout the domain. Hence, an adaptive Lagrangian–Eulerian approach on unstructured grids seems to be the best way of enhancing the present scheme by reducing the total number of grid nodes and degrees of freedom of the system and, consequently, the total computational time necessary to achieve the final solution. Future work will focus on these ideas.

ACKNOWLEDGEMENTS

The authors acknowledge the financial support from Conselho Nacional de Desenvolvimento Científico e Tecnológico, CNPq, and Coordenação de Aperfeiçoamento de Pessoal de Nível Superior, CAPES. A large portion of this work has been carried out during the stay of the first author at Laboratoire de Combustion et de Détonique (Poitiers, France) in the framework of a 'co-tutelle' thesis prepared under the co-supervision of University of Poitiers and Instituto Tecnológico de Aeronáutica (ITA). The authors further acknowledge the partial support of CNPq under the Integrated Project Research Grant No. 522.413/96-0. The authors thank the contribution of Dr Márcio Teixeira de Mendonça of ASA-P on the revision of this text.

REFERENCES

1. Karki KC, Patankar SV. Pressure based calculation procedure for viscous flows at all speeds in arbitrary configurations. *AIAA Journal* 1989; **27**(9):1167–1174.
2. Chen K-H, Pletcher RH. Primitive variable, strongly implicit calculation procedure for viscous flows at all speed. *AIAA Journal* 1991; **29**(8):1241–1249.
3. Chorin AJ. A numerical method for solving incompressible viscous flow problems. *Journal of Computational Physics* 1967; **2**:12–26.
4. Bruel P, Karmed D, Champion M. A pseudo-compressibility method for reactive flows at zero Mach number. *International Journal of Computational Fluid Dynamics* 1996; **7**:291–310.
5. Corvellec C. Numerical and analytical study of a combustion zone propagating characteristics developing on premixed turbulent flow modelised by a flamelet approach type. *Ph.D. Thesis*, Université de Poitiers—Ecole Nationale Supérieure de Mécanique et d'Aérotechnique (ENSMA), December 1998 (in French, original title is 'Étude Numérique et Analytique des Caractéristiques Propagatives d'une Zone de Combustion se Développant au Sein d'un Écoulement Turbulent Prémélangé Modélisée par une Approche de Type *Flammelette*').
6. Corvellec C, Bruel P, Sabel'nikov VA. A time-accurate scheme for the calculations of unsteady reactive flows at low Mach number. *International Journal for Numerical Methods in Fluids* 1999; **29**:207–227.
7. Dourado WMC, Azevedo JLF. Flow simulation with unstructured meshes over basic automotive configurations with all-speed method. In *Proceedings of the 6th Brazilian Congress of Engineering and Thermal Sciences and 6th Latin American of Mass and Heat Transfer*, *ENCIT/LATCYM 96*, vol. I. Florianópolis, SC, November 1996; 553–558 (in Portuguese, original title is 'Simulação de Escoamentos com Malhas Não-Estruturadas sobre Configurações Automotivas Básicas com um Método para Toda a Faixa de Velocidade').

8. Dourado WMC, Azevedo JLF. Analysis of an all-speed method in laminar flows using unstructured meshes. In *Proceedings of the 15th Brazilian Congress of Mechanical Engineering*, Águas de Lindóia, SP, Brazil, November 1999.
9. Dourado WMC, Azevedo JLF, Bruel P. Application of the all-speed method to steady and unsteady flows on unstructured grids. In *Proceedings of the 8th Brazilian Congress of Thermal Engineering and Sciences*, Porto Alegre, RS, Brazil, October 2000.
10. Jameson A, Baker TJ, Weatherill NP. Calculation of inviscid transonic flow over a complete aircraft. In *Proceedings of the 24th AIAA Aerospace Sciences Meeting*, number AIAA Paper 86-0103, Reno, NV, January 1986.
11. Barth TJ, Jespersen DC. The design and application of upwind schemes on unstructured meshes. In *Proceedings of the 27th AIAA Aerospace Sciences Meeting*, number AIAA Paper No. 89-0366, Reno, NV, January 1989.
12. Batina JT. Vortex-dominated conical-flow computations using unstructured adaptively refined meshes. In *Proceedings of the 20th AIAA Fluid Dynamics*, *Plasma Dynamics and Lasers Conference*, number AIAA Paper No. 89-1816, Buffalo, NY, June 1989.
13. Trépanier JY, Reggio M, Zhang H, Camarero R. A finite-volume method for the Euler equations on arbitrary Lagrangian–Eulerian grids. *Computers and Fluids* 1991; **20**(4):399–409.
14. Nomura T, Hughes TJR. An arbitrary Lagrangian–Eulerian finite element method for interaction of fluid and rigid body. *Computer Methods in Applied Mechanics and Engineering* 1992; **95**:115–138.
15. Bray KNC, Moss JB. A unified statistical model of the premixed turbulent flame. *Acta Astronautica* 1977; **4**:291–319.
16. Bray KNC, Libby PA, Moss JB. Flamelet crossing frequencies and mean reaction rates in premixed turbulent combustion. *Combustion Science and Technology* 1984; **41**:143–172.
17. Bray KNC, Champion M, Libby PA. Mean reaction rates in premixed turbulent flames. In *Proceedings of the 22nd Symposium* (*International*) *on Combustion*, The Combustion Institute, 1988, 763–769.
18. Champion M, Libby PA. Turbulent premixed combustion in a boundary layer. *Combustion Science and Technology* 1984; **38**:267–291.
19. Majda AJ, Sethian J. The derivation and numerical solution of the equations for zero Mach number combustion. *Combustion Science and Technology* 1985; **42**:185–205.
20. Favre A. Compressible turbulent gas equations. *Journals de Mécanique* 1965; **4**:361–391 (in French, original title is 'Equations des Gaz Turbulents Compressibles').
21. Sabel'nikov VA, Corvellec C, Bruel P. Analysis of the influence of cold front quenching on the turbulent burning velocity associated with an eddy break-up model. *Combustion and Flame* 1998; **113**:492–497.
22. Kolmogorov A, Petrovsky I, Piscounov N. Study of the diffusion equation with growth of the quantity of matter and its application to a biology problem. *Bulletin of The Moscow State University*, *International Series*, vol. 1, Section A(6), 1937.
23. Zeldovich YB, Barenblatt GI, Librovich VB, Makhviladze GM. *The Mathematical Theory of Combustion and Explosions*. Consultants Bureau—Plenum Publishing Corporation, New York, NY, 1985.
24. Bray KNC, Libby PA. Interaction effects in turbulent premixed flames. *The Physics of Fluids* 1976; **19**(11):1687–1701.
25. Catlin CA, Lindstedt RP. Premixed turbulent burning velocities derived from mixing controlled reaction models with cold front quenching. *Combustion and Flame* 1991; **85**:427–439.
26. Soh WY, Goodrich JM. Unsteady solution of incompressible Navier–Stokes equations. *Journal of Computational Physics* 1988; **79**:113–134.
27. Chang JLC, Kwak D. On the method of pseudo-compressibility for numerically solving incompressible flows. Number 84-0252, AIAA, 1984.
28. Rogers SE, Kwak D. An upwind differencing scheme for the time-accurate incompressible Navier–Stokes equations. *AIAA Journal* 1990; **28**(2):253–262.
29. Rogers SE, Kwak D, Kiris C. Steady and unsteady solutions of the incompressible Navier–Stokes equations. *AIAA Journal* 1991; **29**(4):603–607.
30. Frisch U. *Turbulence*. Cambridge University Press: Cambridge, MA; 1995.
31. Launder BE, Spalding DB. The numerical computational of turbulent flows. *Computer Methods in Applied Mechanics and Engineering* 1974; **3**:269–289.
32. Mavriplis DJ, Jameson A, Martinelli L. Multigrid solution of the Navier–Stokes equations on triangular meshes. *NASA CR*- 89-11, Institute for Computer Applications in Science and Engineering (ICASE), NASA Langley Research Center, Hampton, VA, February 1989.
33. Mavriplis DJ. Accurate multigrid solution of the Euler equations on unstructured and adaptative meshes. *AIAA Journal* 1990; **28**(2):213–221.
34. van Leer B. Towards the ultimate conservative difference scheme III. Upstream-centered finite-diference scheme for ideal compressible flow. *Journal of Computational Physics* 1977; **23**:263–275.
35. van Leer B. Towards the ultimate conservative difference scheme IV. A new approach to numerical convection. *Journal of Computational Physics* 1977; **23**:276–299.

36. Roe PL. Approximate Riemman solvers, parameter vectors, and difference schemes. *Journal of Computational Physics* 1981; **43**:357–372.
37. van Leer B, Thomas JL, Roe PL, Newsome RW. A comparison of numerical flux formulas for the Euler and Navier–Stokes equations. In *Proceedings of the 8th AIAA Computational Fluid Dynamics Conference*, number AIAA Paper No. 87-1104, June 1987.
38. Löhner R, Morgan K, Peraire J, Vahdati M. Finite-element flux-corrected transport for the Euler and Navier–Stokes equations. *ICASE Report* 87-4, Institute for Computer Applications in Science and Engineering—ICASE, NASA Langley Research Center, Hampton, VA, January 1987.
39. Mavriplis DJ, Venkatakrishnan V. A unified multigrid solver for the Navier–Stokes equations on mixed element meshes. *ICASE Report* 95-53, Institute for Computer Applications in Science and Engineering (ICASE), NASA Langley Research Center, Hampton, VA, July 1995.
40. Mavriplis DJ. Multigrid strategies for viscous flow solvers on anisotropic unstructured meshes. *ICASE Report* 98-6, Institute for Computer Applications in Science and Engineering—ICASE, NASA Langley Research Center, Hampton, VA, January 1998.
41. Manzari MT, Hassan O, Morgan K, Weatherill NP. Turbulent flow computation on 3D unstructured grids. *Finite Elements in Analysis and Design* 1998; **30**:353–363.

